Effect of anisotropy on small magnetic clusters

Alfred Hucht[1], Sanjubala Sahoo[1], Shreekantha Sil[2], and Peter Entel[1]
[1] *Faculty of Physics and Center for Nanointegration CeNIDE, University of Duisburg–Essen, 47048 Duisburg, Germany*
[2] *Department of Physics, Visva Bharati University, Santiniketan, 731235 West Bengal, India*
(Dated: August 31, 2011)

The effect of dipolar interaction and local uniaxial anisotropy on the magnetic response of small spin clusters where spins are located on the vertices of icosahedron (I_h), cuboctahedron (O_h), tetrahedron (T_h) and square geometry have been investigated. We consider the ferromagnetic and antiferromagnetic spin-1/2 and spin-1 Heisenberg model with uniaxial anisotropy and dipolar interaction and apply numerical exact diagonalization technique in order to study the influence of frustration and anisotropy on the ground state properties of the spin-clusters. The ground state magnetization, spin-spin correlation and several thermodynamic quantities such as entropy and specific heat are calculated as a function of temperature and magnetic field.

I. INTRODUCTION

Realizing the promising applications in physics, magnetochemistry and biomedicine, molecular magnets have recently been the focal point of intense subject of research. Although these materials appear as macroscopic objects, i.e., crystals or powders, the intramolecular magnetic interactions are utterly negligible as compared to the intramolecular interaction. Thus their magnetic properties mainly reflect the ensemble properties of small clusters. It appears that in majority of these molecules, the localized single particle magnetic moments couple antiferromagnetically and the spectrum is rather well described by the Heisenberg model with isotropic nearest neighbor interaction, sometimes augmented by anisotropic terms and dipolar interactions[1–7]. Thus, the interest in the Heisenberg model, which is known for a long time, is renewed recently by the successful synthesis of new magnetic clusters and magnetic molecules.

Ab initio studies show that often these magnetic systems are frustrated due to the competing magnetic interactions between the individual magnetic moments. The effect of finite sizes, quantum fluctuations and frustrations can have dramatic consequences on the energy spectra and can even give rise to new phases apart from the conventional Néel-like order[7–21]. A great deal of effort has been devoted to the theoretical studies on magnetic clusters using different theoretical techniques to solve the Heisenberg model[8,11,22,23].

Using exact diagonalization of the antiferromagnetic Heisenberg model, Konstantinidis *et al.*[8] have calculated the ground state magnetization for a dodecahedron and icosahedron symmetry for $s = 1/2$ and 1 and have obtained discontinuity in the field-dependent magnetization and double peaks in the temperature-dependent specific heat arising due to frustrations. Using perturbation theory, Coffey *et al.*[22] have studied the effect of frustration and connectivity on the magnetic properties of a 60-site cluster. Schnalle *et al.*[11] have applied an approximation of diagonalization scheme to a cuboctahedron for $s = 1$ and 3/2 in order to obtain the energy spectra. In addition to the magnetic properties, several studies exist for the thermodynamic properties of clusters. For example, Honecker *et al.*[23] have calculated several magnetothermal properties such as the magnetic susceptibility, specific heat and magnetic cooling rate for a cuboctahedron with different spin quantum numbers using the antiferromagnetic Heisenberg model. Besides the exact diagonalization method, several other techniques such as the density matrix renormalization group[24,25], cluster expansions[26], spin-wave expansions[27–29] and quantum Monte Carlo techniques[30–32] can be used to study the magnetic systems. However, some of these techniques have drawbacks, for example, quantum Monte Carlo technique has limitations in describing the systems with geometric frustration. The advantage of exact diagonalization method relative to these approximate methods is that one obtains all informations about the whole energy spectra such as the degeneracy, the lowest eigenenergies and eigenfunctions from which the ground state as well as finite temperature properties can be calculated.

In the present work we have applied the exact diagonalization method to calculate the properties of clusters with spin-1/2 and 1. We have studied the magnetic and thermodynamic properties of small clusters with the focus on showing the effect of dipolar interaction and uniaxial anisotropy on the magnetization behavior in the presence of magnetic field, the studies of which are still limited in literature[33–35]. In addition, the temperature-dependent as well as the ground state spin-spin correlation functions are calculated for these clusters and are compared with respect to the classical case.

The paper is organized as follows: In section II, we describe the theoretical method used for modeling the quantum clusters. Section III discusses the results obtained for 13-atom clusters with spin-1/2, including the effect of dipolar interaction. Then, section IV describes the findings for 4-atom clusters with spin-1, where the effect of uniaxial anisotropies and temperature-dependent correlation functions has been discussed, and section V discusses the results for spin-1 icosahedron in the presence of local uniaxial anisotropies. In section VI the results are summarized.

II. THEORETICAL METHOD

From first-principles calculations it turns out[36] that the interaction between electrons may be well represented by a model Hamiltonian describing a set of interacting spins $\vec{s}_i$. An important class of such interacting spin models consists of spins coupled bilinearly on a finite lattice. The Hamiltonian of such a system can be expressed by Heisenberg Hamiltonian,

$$\mathcal{H}_0 = -\sum_{i<j} J_{ij}\, \vec{s}_i \cdot \vec{s}_j, \tag{1}$$

where in general the sum runs over all pairs. $\vec{s}_i$ is the spin operator on site i having total spin s and z component of the spin $\vec{s}_i$ can take values $s_i^z = -s, -s+1, \ldots, s$; J_{ij} is the exchange interaction. This model describes the ferromagnetic (antiferromagnetic) Heisenberg model when $J_{ij} > 0$ ($J_{ij} < 0$). In one dimension and for only nearest-neighbor couplings $J_{ij} = J$, the s=1/2 Heisenberg model has been solved analytically by means of the Bethe *ansatz*[37]. Unfortunately, the use of the Bethe *ansatz* is quite limited, as this method is only applicable to models in one dimension. For higher dimensions, one has to look for approximate methods. When the number of spins in the system is small enough, one can solve the problem by employing exact diagonalization techniques[38]. A straightforward way to study the model Hamiltonian, defined in Eq. (1), numerically is simply to obtain the matrix elements of $\mathcal{H}$ in a basis of $|s_1^z, s_2^z, \ldots, s_n^z\rangle$, with the z-axis taken as quantization direction, where n is the total number of spins in the system, and then diagonalize the Hamiltonian matrix numerically. The Hamiltonian matrix can be decomposed into block structure with the use of symmetries of the model. Since the isotropic Heisenberg model includes only the scalar product between the spins, the Hamiltonian is rotationally invariant in spin space, i.e., it commutes with the square of the total spin of the system, S^2 and the z component of the total spin, S^z. Even though it is straightforward to work in a S^z subspace, there is no simple method to construct symmetry adopted eigenstates of $\vec{S}^2$. Construction of symmetry adopted eigenstates of $\vec{S}^2$ requires more involved calculations[39–43]. Additionally, the Hamiltonian is symmetric under permutations of spins that respect the connectivity of our small sized cluster, and the model possesses time reversal symmetry in the absence of external magnetic fields. When we take into account the symmetries in the system, the S^z basis states can be projected onto states that transform under specific irreducible representation of the symmetry group. In this way, the Hamiltonian is block diagonalized into smaller matrices and the maximum dimension required for numerical diagonalization is considerably reduced compared to full Hilbert space size.

In the presence of an external magnetic field, dipolar interaction and anisotropy the Heisenberg Hamiltonian (1) is modified to

$$\mathcal{H} = \mathcal{H}_0 - B^z S^z + \mathcal{H}_{\rm dipole} + \mathcal{H}_{\rm ani} \tag{2}$$

where B^z is the homogeneous external magnetic field defining, without loss of generality, the z-direction. Here it may be noted that the factor $g\mu_B$ is absorbed into B^z and z component of the the total spin, $S^z = \sum_i s_i^z$, can take values from $-S$ to S in unit steps, where S is the maximum total spin of the system. The dipolar term $\mathcal{H}_{\rm dipole}$ in Eq. (2) is defined as

$$\mathcal{H}_{\rm dipole} = \frac{\mu_0}{4\pi}(g\mu_{\rm B})^2 \sum_{i<j} \frac{\vec{s}_i \cdot \vec{s}_j - 3(\vec{s}_i \cdot \hat{\vec{r}}_{ij})(\hat{\vec{r}}_{ij} \cdot \vec{s}_j)}{|\vec{r}_{ij}|^3} \tag{3}$$

where $\hat{\vec{r}}_{ij} = \vec{r}_{ij}/|\vec{r}_{ij}|$ is the unit vector along the line connecting the two spins or dipoles located on the sites i and j, and the sum runs over all pairs. $\mathcal{H}_{\rm ani}$ in Eq. (2) represents the local uniaxial anisotropy, which is defined by

$$\mathcal{H}_{\rm ani} = -\sum_i D_i\, (\vec{e}_i \cdot \vec{s}_i)^2 \tag{4}$$

where D_i are the local uniaxial anisotropy constants and $\vec{e}_i$ is the unit vector giving the radial direction from the central spin. Since the commutators, $[\mathcal{H}_{\rm dipole}, S^z] \neq 0$ and $[\mathcal{H}_{\rm ani}, S^z] \neq 0$, S^z is no-more a good quantum number in presence of dipolar interaction $\mathcal{H}_{\rm dipole}$ or anisotropy term $\mathcal{H}_{\rm ani}$ and therefore in presence of dipolar or anisotropy term the block diagonalization with respect to different S^z values is not possible.

Now we construct the Hamiltonian matrix in terms of eigenstates of the total S^z operator and express the Hamiltonian in terms of the raising and lowering operators $s_i^{\pm} = s_i^x \pm i s_i^y$. When s_i^+ and s_i^- operates on the eigenstates of s_i^z, we have

$$s_i^{\pm}|s_i^z\rangle = \sqrt{s(s+1) - s_i^z(s_i^z \pm 1)}\, |s_i^z \pm 1\rangle. \tag{5}$$

For example, for a spin-1/2 particle,

$$s_i^+|\uparrow_i\rangle = 0,\ s_i^+|\downarrow_i\rangle = |\uparrow_i\rangle,$$
$$s_i^-|\uparrow_i\rangle = |\downarrow_i\rangle,\ s_i^-|\downarrow_i\rangle = 0,$$

and for a spin-1 particle,

$$s_i^+|\uparrow_i\rangle = 0,\ s_i^+|0_i\rangle = \sqrt{2}|\uparrow_i\rangle,$$
$$s_i^+|\downarrow_i\rangle = \sqrt{2}|0_i\rangle,\ s_i^-|\uparrow_i\rangle = \sqrt{2}|0_i\rangle,$$
$$s_i^-|0_i\rangle = \sqrt{2}|\downarrow_i\rangle, s_i^-|\downarrow_i\rangle = 0,$$

where in the latter case $\{\downarrow, 0, \uparrow\}$ denote the three possible values of $s_i^z = -1, 0, 1$. In the absence of $\mathcal{H}_{\rm dipole}$ and $\mathcal{H}_{\rm ani}$, the z component of the total spin is a conserved quantity and we can decompose the Hamiltonian matrix into smaller blocks characterizing each values of the total spin. For example, in case of a 13-atom cluster with $s = 1/2$, the $2^{13} \times 2^{13}$ dimensional Hamiltonian matrix

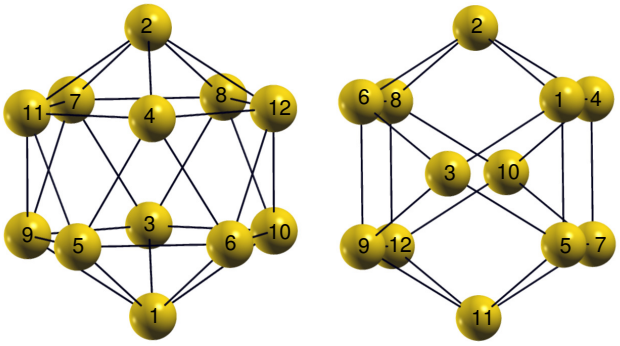

FIG. 1. (Color online) Schematic picture of ICO (left) and CUBO (right) with labeling of each atomic site. Both structures have 12 vertices with one atom at center (not shown). The magnetic field is aligned parallel to $\vec{r}_2$ for both ICO and CUBO.

is divided into blocks with dimension $\binom{13}{k} \times \binom{13}{k}$, with $k = 0, \ldots, 13$. 14 such block matrices have to be diagonalized and the largest block matrix has $\binom{13}{6} = 1716$ rows. It may be noted that S^z being the good quantum number, the Zeeman term is not needed to be included in numerical diagonalization process and can be included later by shifting the eigenvalues by $B^z S^z$. However, these simplification is not possible when dipolar interaction or uniaxial anisotropy term is present in the Hamiltonian.

III. 13-ATOM CLUSTERS WITH $s = 1/2$

We have considered two different geometries, namely icosahedron (ICO) and cuboctahedron (CUBO) for the investigation of 13-atom clusters. The characteristic feature of the icosahedron, which has a connectivity like fullerenes[44,45], is that it possesses 12 vertices, 20 triangular faces and 30 edges. It is categorized in the symmetry group of I_h, which is the point symmetry group with 120 operations[46]. On the other hand, a cuboctahedron has 12 vertices with 8 triangular and 6 square faces and 24 identical edges, and belongs to the symmetry group O_h. Schematic pictures of the ICO and CUBO geometry are shown in the left and right panel of Fig. 1, respectively. Both geometries possess 12 vertices on the surface shell and one atom at the center, and can be transformed into each other via a Mackay transformation[47]. Though the number of nearest neighbors for the center atom are same (12) for both geometries, each of the surface atoms for both cases possesses different number of nearest neighbors, i.e., the ICO has 5 and the CUBO has 4 nearest neighbors in the outer shell. In this section we first study the ground state properties and thermodynamic quantities like entropy and specific heat in the absence of dipolar and uniaxial anisotropy term and then switch on the dipolar interaction to investigate its influence on ground state properties.

In the absence of $\mathcal{H}_{\rm dipole}$ and $\mathcal{H}_{\rm ani}$, the total Hamiltonian for a 13-atom cluster with nearest-neighbor interaction can be written as

$$\mathcal{H}_{13} = -J \sum_{\substack{i,j>0 \\ \langle ij \rangle}} \vec{s}_i \cdot \vec{s}_j - J' \sum_{i>0} \vec{s}_0 \cdot \vec{s}_i - B^z \sum_i s_i^z \qquad (6)$$

where $\vec{s}_0$ is the spin of the center atom, and the first sum runs over all nearest-neighbor pairs $\langle ij \rangle$ in the surface shell. J is the exchange coupling between atoms in the surface shell and J' is the exchange coupling between central and surface spins.

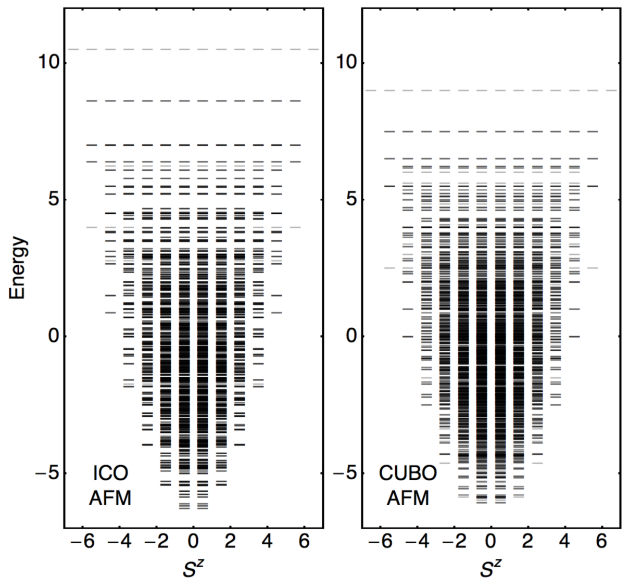

FIG. 2. All 8192 energy eigenvalues in units of $|J|$ for AFM interactions of the 13-atom ICO (left panel) and CUBO (right panel) with spin-1/2. The energy levels are shaded according to their degeneracy. There exists a $\pm S^z$ degeneracy in the AFM case for both symmetries. For the FM case, the energy spectra are reversed with respect to the AFM spectra which fulfills $\mathrm{E_{FM}} = -\mathrm{E_{AFM}}$.

The energy spectrum for the two clusters namely the ICO and the CUBO clusters can be obtained by diagonalizing the above Hamiltonian. In the presence of magnetic field the ground state energy is obtained by considering the minimum of the energy eigenvalues from each magnetization sector. We have calculated the energy eigenvalues for the different exchange couplings defined by (i) all spins ferromagnetic ($J = J' = 1$), (ii) all spins antiferromagnetic ($J = J' = -1$), (iii) central spin is reversed with respect to the ferromagnetic surface ones ($J = 1$ and $J' = -1$), (iv) antiferromagnetic surface spins with ferromagnetic central spin ($J = -1$ and $J' = 1$). However, we will mainly discuss the ferromagnetic ($J = J' = 1$) and antiferromagnetic ($J = J' = -1$) cases. Note that all energies are measured in units of $|J|$ with $|J|$ is fixed to the value 1 in this work.

In Table I we present closed form expressions for the ground state energies E_0, degeneracies K_0, as well as the lowest energy gap ΔE_1 for the different S^z sectors of

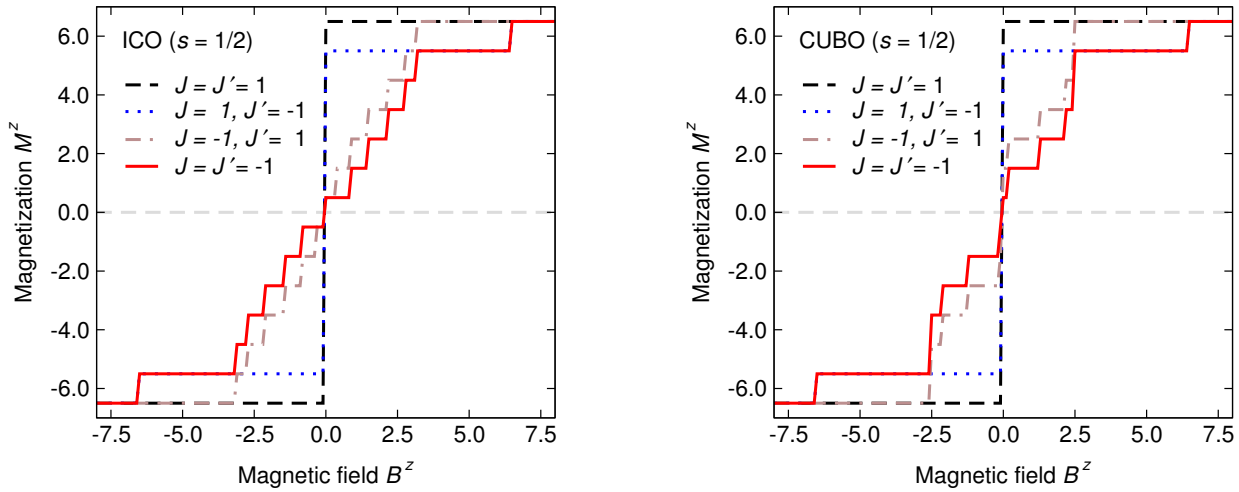

FIG. 3. (Color online) Variation of magnetization $M^z = \langle S^z \rangle$ as a function of the magnetic field for four different exchange interactions as listed in the panels of ICO (left panel) and CUBO (right panel). J and J' are the exchange couplings among the surface spins and center-surface spins, respectively. The external magnetic field is measured in units of $|J|$.

ICO and CUBO. The exact polynomials are determined with the *Mathematica* routine "RootApproximant"[48] using high precision arithmetics with up to 400 digits. Due to the two-fold degeneracy for the $\pm S^z$ sector, where the minimum energy for each positive S^z sector has the same value as that of the corresponding negative S^z sector, we have listed the results as function of $|S^z|$ only.

The whole eigenvalue spectrum in the absence of external magnetic field is depicted in Fig. 2 for the AFM interactions of ICO (left panel) and CUBO (right panel), where the minimum energy eigenvalues for different magnetization of the system are found to be different. More over the energy gaps between the minimum energy eigenvalues of the consecutive S^z sectors differ for both ICO and CUBO. This observation identifies the influence of symmetry on the nature of eigenvalue spectrum of the system and also explains the nature of the variation of the magnetization with respect to the external magnetic field for the two clusters. For the FM interaction, we obtain degenerate minimum energies. This occurs because of the fact that the Hamiltonian has spin rotational invariance and as a result, turning the total spin in another direction does not change the energy of the system.

TABLE I. Lowest energy eigenvalue E_0, degeneracy K_0 and lowest energy excitation $\Delta E_1 = E_1 - E_0$ for different S^z for 13-atom AFM ICO and CUBO. Energies are in units of $|J|$.

$\|S^z\|$	$E_0^{\rm ICO}$	$K_0^{\rm ICO}$	$\Delta E_1^{\rm ICO}$	$E_0^{\rm CUBO}$	$K_0^{\rm CUBO}$	$\Delta E_1^{\rm CUBO}$
13/2	21/2	1	–	9	1	–
11/2	4	1	2.382	5/2	1	3
9/2	$2-\sqrt{5}/2$	3	0.618	0	5	1
7/2	-1.834[a]	5	0.102	$-5/2$	3	0.293
5/2	-3.967[b]	4	0.0045	-4.631[c]	1	0.339
3/2	-5.420[d]	5	0.022	-5.869[e]	1	0.093
1/2	-6.288[f]	3	0.100	-6.062[g]	3	0.093

[a] Zero of $x^3 - 5x - 3 = 0$

[b] Zero of $64x^6 + 448x^5 + 656x^4 - 1184x^3 - 3412x^2 - 2036x - 53 = 0$

[c] Zero of $2x^5 + 16x^4 + 29x^3 - 23x^2 - 61x - 8 = 0$

[d] Zero of $4x^{10} + 84x^9 + 700x^8 + 2842x^7 + 4992x^6 - 1726x^5 - 21401x^4 - 31503x^3 - 14082x^2 + 4014x + 3402 = 0$

[e] Zero of $64x^6 + 960x^5 + 4784x^4 + 7168x^3 - 8148x^2 - 19868x + 6361 = 0$

[f] Zero of $65536x^{16} + 2752512x^{15} + 51707904x^{14} + 571146240x^{13} + 4089167872x^{12} + 19595452416x^{11} + 61510348800x^{10} + 109531144192x^9 + 14047096320x^8 - 488888621568x^7 - 1389656886528x^6 - 2016792866048x^5 - 1655926247744x^4 - 669806791648x^3 - 39673588208x^2 + 46200676992x + 7484904361 = 0$

[g] Zero of $64x^{21} + 3136x^{20} + 70272x^{19} + 952256x^{18} + 8684000x^{17} + 55985680x^{16} + 259611872x^{15} + 853909520x^{14} + 1844888624x^{13} + 1761797108x^{12} - 3621087792x^{11} - 18691236512x^{10} - 39464764094x^9 - 49351650308x^8 - 34081746286x^7 - 3226424608x^6 + 17175800242x^5 + 16425687591x^4 + 6952269434x^3 + 1297049762x^2 + 47065144x - 4927905 = 0$

The left panel of Fig. 3 shows the variation of magnetization in the unit of $g\mu_B$ as a function of external magnetic field for the four cases of interactions of the ICO (mentioned above). In the presence of an external magnetic field, the minimum energy configuration for the AFM interaction ($J = J' = -1$) gives rise to plateaus, which have been marked by the solid red curve in the left panel of Fig. 3. The appearance of different sizes of plateaus is related to the inequivalent energy gaps between the minimum energy values of consecutive S^z sectors. On the other hand for FM interaction the ground state energy lies in the $S^z = 13/2$ sector for all positive values of B^z and in the $S^z = -13/2$ sector for all negative values of B^z. Thus for the ferromagnetic interaction ($J = J'$), irrespective of the values of magnetic field, $|M^z| = 13/2$ (see the black dashed line in Fig. 3). The right panel of Fig. 3 shows the variation of magnetization as a function of magnetic field for the four different set of exchange couplings in the case of CUBO geometry. As observed in the case of ICO, a similar behavior for the variation of magnetization with respect to the external magnetic field is observed for the FM interaction. How-

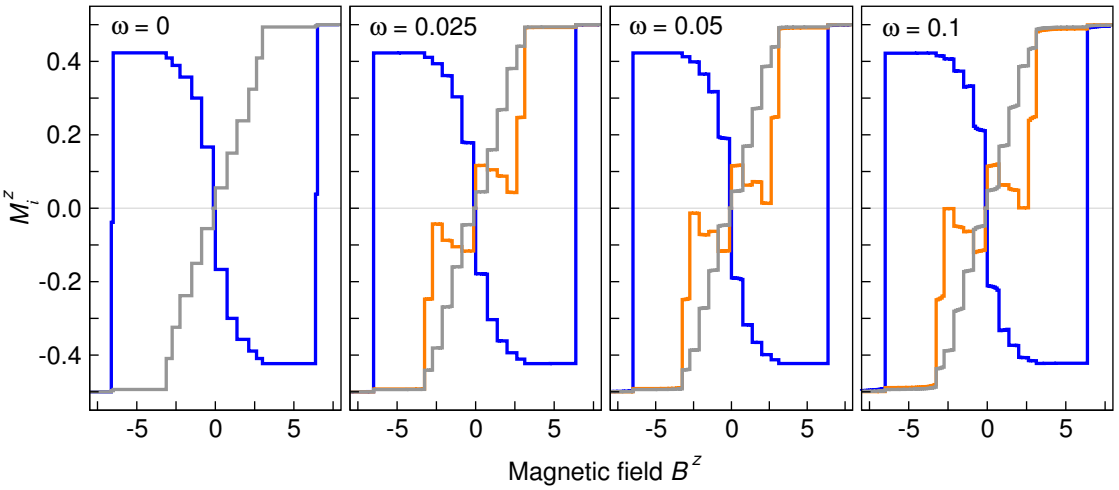

FIG. 4. (Color online) Variation of ground state magnetization $M_i^z = \langle s_i^z \rangle$ as a function of magnetic field (in units of $|J|$) for the AFM case of 13-atom ICO at several values of the reduced dipole coupling strengths ω. The dark blue lines in all plots show the field-dependence of magnetization for the center spin $\langle s_0^z \rangle$. The orange and light gray lines show the same quantity for the top/bottom atoms and remaining 10 atoms on the surface, respectively. The top/bottom spins are strongly affected by dipolar interactions.

ever, for the AFM interactions of CUBO, the plateaus appearing in the magnetization have different sizes compared to the ICO, which can be noted from the solid red curve in the right panel of Fig. 3. The differences in results is the consequence of the differences in structural symmetries of the two clusters.

Now we shall study the effect of dipolar interaction on the magnetization of the 13 atom ICO with $s = 1/2$ in presence of magnetic field. Since dipolar interaction breaks the isotropy of the system, dipole-dipole interaction may be an important source of the observed magnetic anisotropy of various magnetic materials[49]. Moreover, as dipole-dipole coupling depends only on known physical constants and inverse cube of the interatomic distances, understanding the role of dipolar interaction on different properties of the molecule will be useful in the studies of molecular structures. For our studies we shall consider the Hamiltonian given in Eq. (3). Using the exact diagonalization technique we calculate the magnetic properties of the above mentioned system. Figure 4 shows the variation of magnetization as a function of the magnetic field for different reduced dipolar interaction strengths,

$$\omega = \frac{\mu_0}{4\pi} \frac{(g\mu_B)^2}{|\vec{r}_{0i}|^3 |J|}, \tag{7}$$

$\omega = 0$, 0.025, 0.05 and 0.1 for the AFM case, where $|\vec{r}_{0i}|$ denotes the shell radius. For $\omega = 0$ we find a reversed central spin $\vec{s}_0$ with negative hysteresis, as long as $B^z/|J'| < 13/2$. For larger fields the central spin flips into field direction. Table II lists the values of center s_0^z and surface spin s_i^z magnetizations for $\omega = 0$ at different values of S^z, given by

$$\langle s_0^z \rangle = -\frac{S^z}{2(S^z+1)}, \qquad \langle s_i^z \rangle = \frac{S^z - \langle s_0^z \rangle}{12}. \tag{8}$$

At finite values of ω, the magnetization of the surface atoms (the light gray curve in Fig. 4) behave differently depending on their position which indicates that the dipolar interaction has a strong impact on the magnetization of these spins. The spins of the top and bottom atoms of the cluster (see left panel of Fig. 1) are strongly modified (orange curves) compared to the other surface spins (light gray) even at very small values of ω, while the magnetization of the center atom is nearly unaffected by the change in ω values. On the other hand, for the FM case, ω has no influence on the magnetization of center or surface spins.

In order to understand the impact of frustration on the spin configuration of the clusters with different geometries, the spin-spin correlation function for ICO and CUBO are also calculated. These are directly connected to the magnetic structure factor by a Fourier transformation, which in principle can be measured experimentally

TABLE II. Ground state expectation values of center and surface spins at $\omega = 0$ for the AFM case of ICO and the corresponding S^z. Note that for $S^z = 13/2$ the central spin is oriented parallel and Eq. (8) does not hold.

S^z	$\langle s_0^z \rangle$	$\langle s_i^z \rangle$
13/2	+0.5000	0.5000
11/2	−0.4231	0.4936
9/2	−0.4091	0.4091
7/2	−0.3889	0.3241
5/2	−0.3571	0.2381
3/2	−0.3000	0.1500
1/2	−0.1667	0.0556

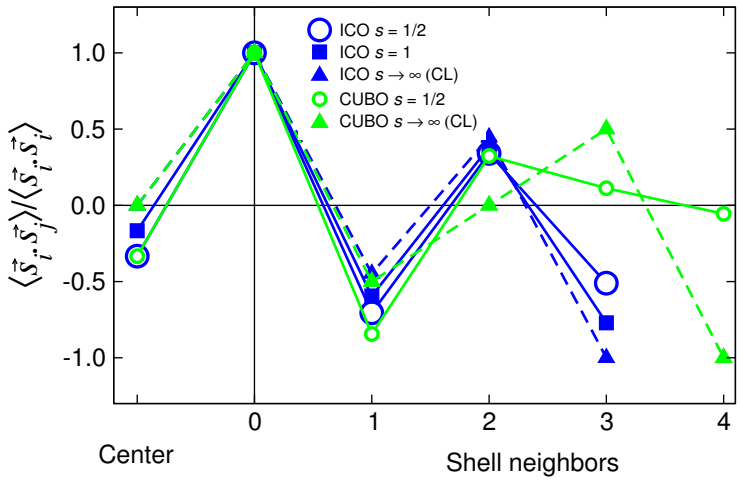

FIG. 5. (Color online) Ground state correlation functions for n^{th} (with $1 \leq n \leq 4$) shell neighbors of ICO and CUBO for the AFM case with spin-1/2 and spin-1. The center and the zero index in the abscissa indicates the correlation functions for the center atom and from center to the atom on surface shell, respectively. The dashed lines indicate the classical limit for spin-∞ ICO and CUBO. For the FM case, the correlation functions for ICO and CUBO with spin-1/2 possess same magnitude (0.25) for all neighbors.

by e.g. neutron scattering techniques. Nevertheless, we are not aware of such experiments on clusters. The correlation function at finite temperature can be defined as

$$\langle \vec{s}_i \cdot \vec{s}_j \rangle = \frac{\mathrm{Tr}\, e^{-\beta \mathcal{H}}\, \vec{s}_i \cdot \vec{s}_j}{\mathrm{Tr}\, e^{-\beta \mathcal{H}}} \tag{9}$$

where, $\beta = 1/T$ with the temperature measured in the units of Boltzmann constant. However, at $T = 0$ the correlation functions are calculated from the eigenvectors obtained from the exact diagonalization of the Hamiltonian in Eq. (6) directly. The distance dependence of the correlation function at zero temperature are plotted in Fig. 5. The correlations for the FM case are found to be the same for both geometries, whereas for AFM interactions, we obtain different correlation functions for ICO and CUBO, suggesting the existence of frustration in the system. However, the ICO seems to be less frustrated with respect to the CUBO, as a regular $+-+-$ oscillation is found for the ICO, while the CUBO exhibits an irregular and smaller correlations in the 3rd and 4th neighbor shell. The ground state correlation functions for the classical limit s$\rightarrow\infty$ are also calculated for these clusters. While comparing the classical and quantum spin correlation functions it reveals that the ground state correlation functions for the ICO with s=1/2 shows a similar qualitative trend compared to the classical case while for the CUBO the correlation functions show large deviations in the third and fourth neighbors relative to the corresponding classical case. This trend indicates that the CUBO has stronger effect of frustration compared to the ICO.

In addition, thermodynamic quantities such as entropy S and specific heat C are calculated in the absence of dipolar or uniaxial terms in Hamiltonian for AFM interactions in the ICO and CUBO as a function of magnetic field at several temperatures, which are shown in Fig. 6. Sharp peaks at low temperature are observed for the AFM case as the magnetic field is changed. This is due to the fact that the thermal fluctuation is enhanced at those magnetic fields where level crossing occurs. With increasing temperature, however, a larger number of states from each S^z sector contributes to the thermodynamics, thereby smearing the peaks of the entropy S is observed. Similar explanation can be given for the behavior of the specific heat with respect to the magnetic field at various temperatures. For the FM case (not shown), however, only the maximum S^z block matrix has the lowest energy for all magnetic fields. In other words, all eigenvalues are simply scaled with magnetic field and thus trivial features observed in the same thermodynamic quantities like S and C and therefore they are not plotted in the present paper. The thermodynamic observables for the antiferromagnetic interactions as a function of temperature for both cluster geometries are shown in Fig. 7. The peak in the specific heat curve as a function of temperature at $T \approx 1$ marks the classical excitations in the system. However, both systems also have pure quantum excitations from the low lying energy levels at lower temperatures, visible as additional peaks in the specific heat and plateaus in the entropy. For example, in the case of ICO at $B^z = 2$, these excitations are at a very low temperature $T \approx 10^{-3}$ and stem from the very small energy gap $\Delta E_1 = 0.0045$ in the $S^z = 5/2$ sector, see Tab. I. A similar behavior is observed at $B^z = 1$, where the maximum at $T \approx 10^{-2}$ comes from the small energy gap $\Delta E_1 = 0.022$ in the $S^z = 3/2$ sector.

Figure 8 shows the variation of magnetization as a function of the magnetic field at different temperatures for AFM (left) and FM (right) interactions, respectively.

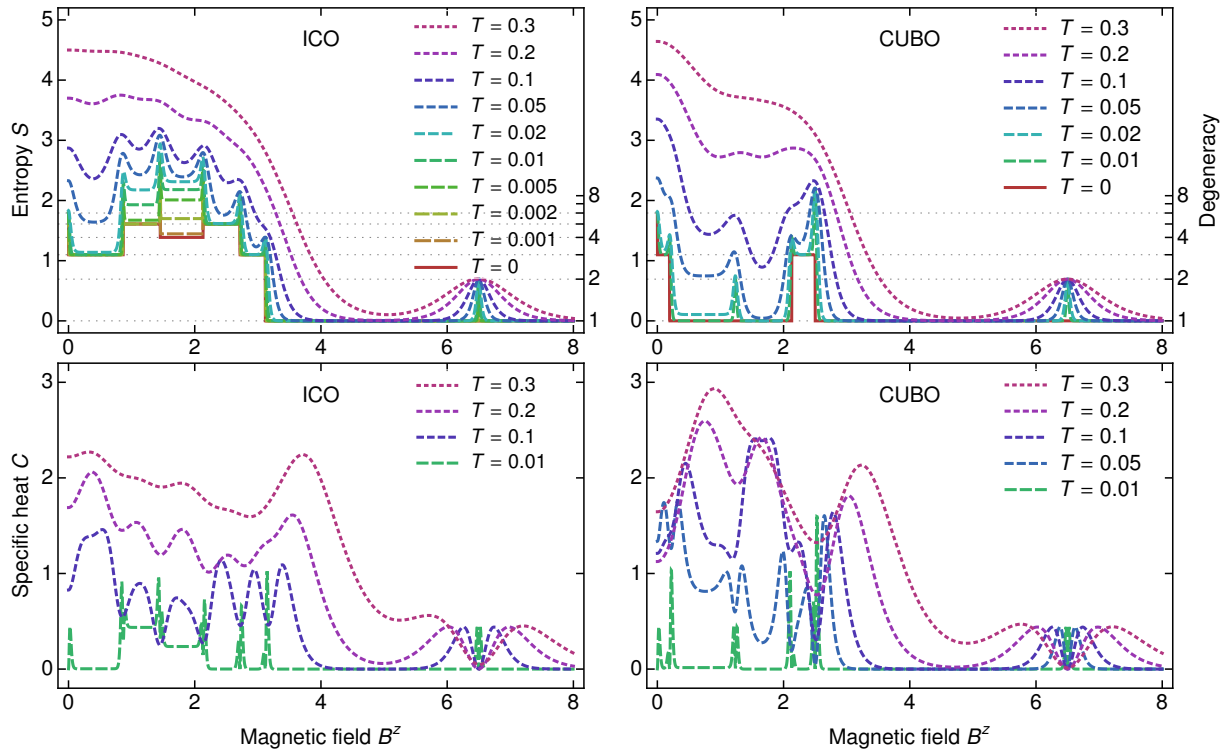

FIG. 6. (Color online) Variation of thermodynamic entities as a function of external magnetic field for the AFM case of 13-atom ICO (left panel) and CUBO (right panel) with spin-1/2. The top and bottom panels show the variation of entropy S and specific heat C with respect to the magnetic field B^z, respectively, at several temperatures T.

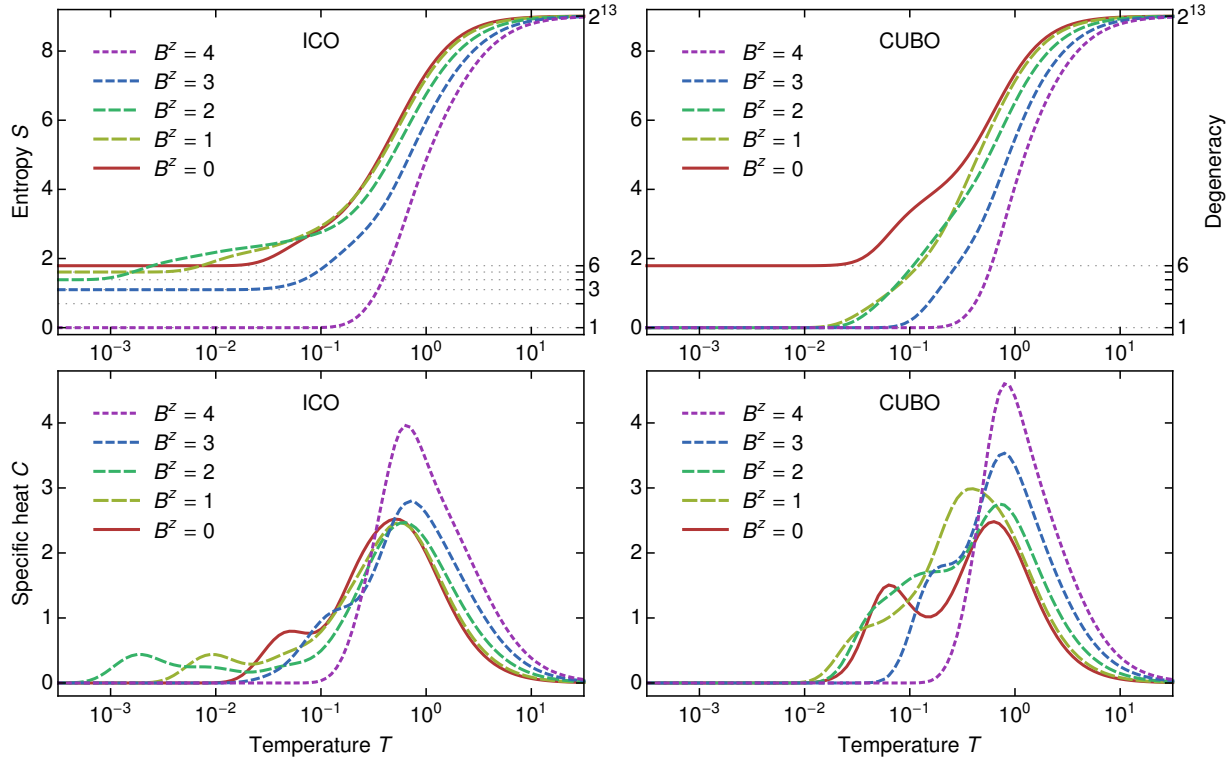

FIG. 7. (Color online) Entropy S (top) and specific heat C (bottom) as a function of temperature (in units of $|J|$) for the AFM case of 13-atom ICO (left panels) and CUBO (right panels) with spin-1/2 for different magnetic fields B^z.

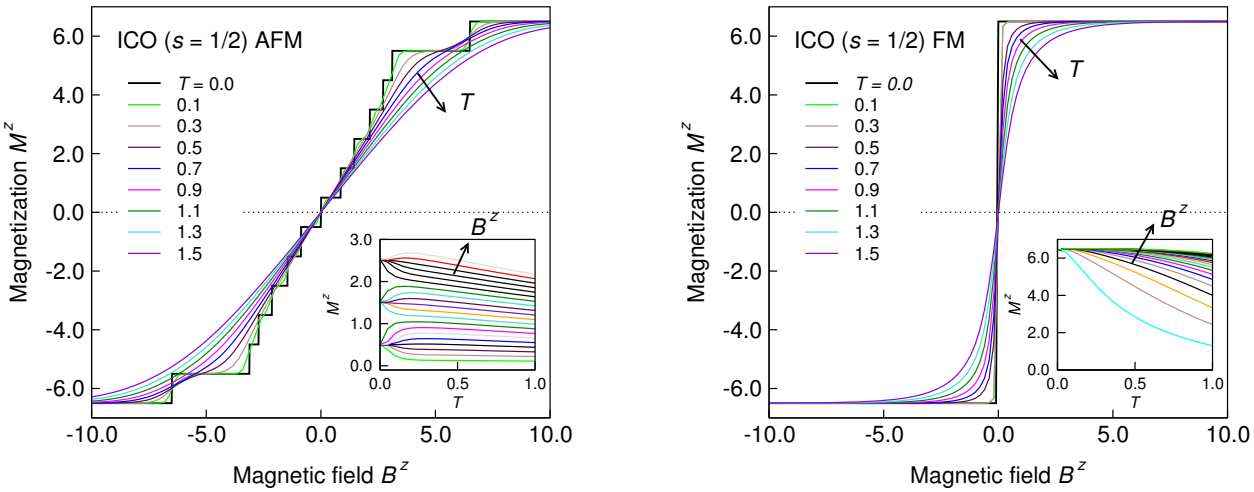

FIG. 8. (Color online) Magnetization as a function of magnetic field measured in units of $|J|$ at various temperatures for the AFM (left) and FM (right) cases of 13-atom ICO. With increase in temperature (arrows), the plateaus start to vanish for the AFM case of 13-atom ICO. The insets for both AFM and FM cases shows the variation of magnetization with respect to temperature for several values of magnetic fields (arrows).

It shows that for both interactions, the magnetization is smeared out with increasing temperature. The insets in Fig. 8 (left and right) show the variation of magnetization with respect to the temperature at different magnetic fields, which shows that quantum effects vanish at around $T \approx 0.1$ in the AFM case and that the total magnetization tends to decrease with increasing temperature. For CUBO, a similar variation of magnetization as a function of magnetic field is observed at several temperatures.

IV. 4-ATOM CLUSTER WITH SPIN-1

Now we present results for 4-atom clusters with $s = 1$ and uniaxial anisotropies (see Eq. (4)). It may be noted

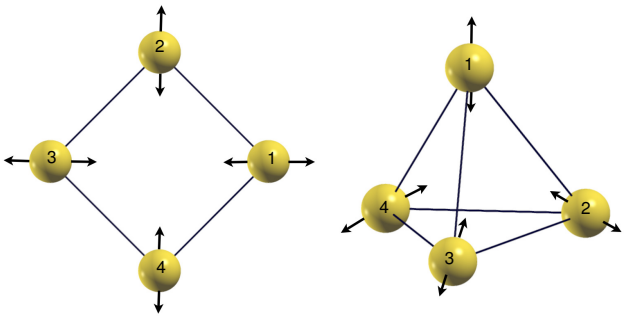

FIG. 9. (Color online) Schematic picture of a planar square (left panel) and a tetrahedron (right panel). The double arrows indicate the radial anisotropy axes for $s = 1$. For the square case, the magnetic field is perpendicular to the plane and for the tetrahedron, it is aligned parallel to $\vec{r}_1$.

that such anisotropies only give a constant for $s = 1/2$. For a spin-1 system, the total Hamiltonian in the presence of local uniaxial anisotropy axes $\vec{e}_i$ reads

$$\mathcal{H}_4 = -\sum_{i<j} J_{ij}\, \vec{s}_i \cdot \vec{s}_j - B^z S^z - \sum_i D_i\, (\vec{e}_i \cdot \vec{s}_i)^2, \quad (10)$$

where D_i are the local uniaxial anisotropy constants and $\vec{e}_i$ are the easy axes compatible with the symmetry of the system[50]. We have previously studied the structural and magnetic properties of small transition metal clusters with more emphasis on the magnetic anisotropy using the density functional theory (DFT)[50], where the energies obtained from DFT calculations were fitted by using a classical Heisenberg Hamiltonian. The investigations presented here can be viewed as a continuation of the previous work in the sense that we perform exact diagonalization of a corresponding quantum spin Hamiltonian to study the system.

There has been several studies related to the magnetic and thermodynamic properties for spin-1 clusters[35,51] through Heisenberg model. However, studies including the effect of local uniaxial anisotropy on several properties of clusters is still limited[52]. In the present work, we have studied the influence of radial anisotropy on the magnetic properties and temperature-dependent correlation functions for the spin-1 tetrahedron and square as shown in Fig. 9. A regular tetrahedron (symmetry group T_d) consists of four triangular faces, whereby the triangles meet at each vertex and are equilateral. A square is a regular quadrilateral with D_4 symmetry.

In the presence of radial anisotropy, the Hamiltonian is modified to a form as represented in Eq. (10), where $D_i = D$ is the anisotropy constant and $\vec{e}_i$ are the easy axes which differs for each spin. In Fig. 9 the anisotropy axes (double arrows) pointing into the radial directions

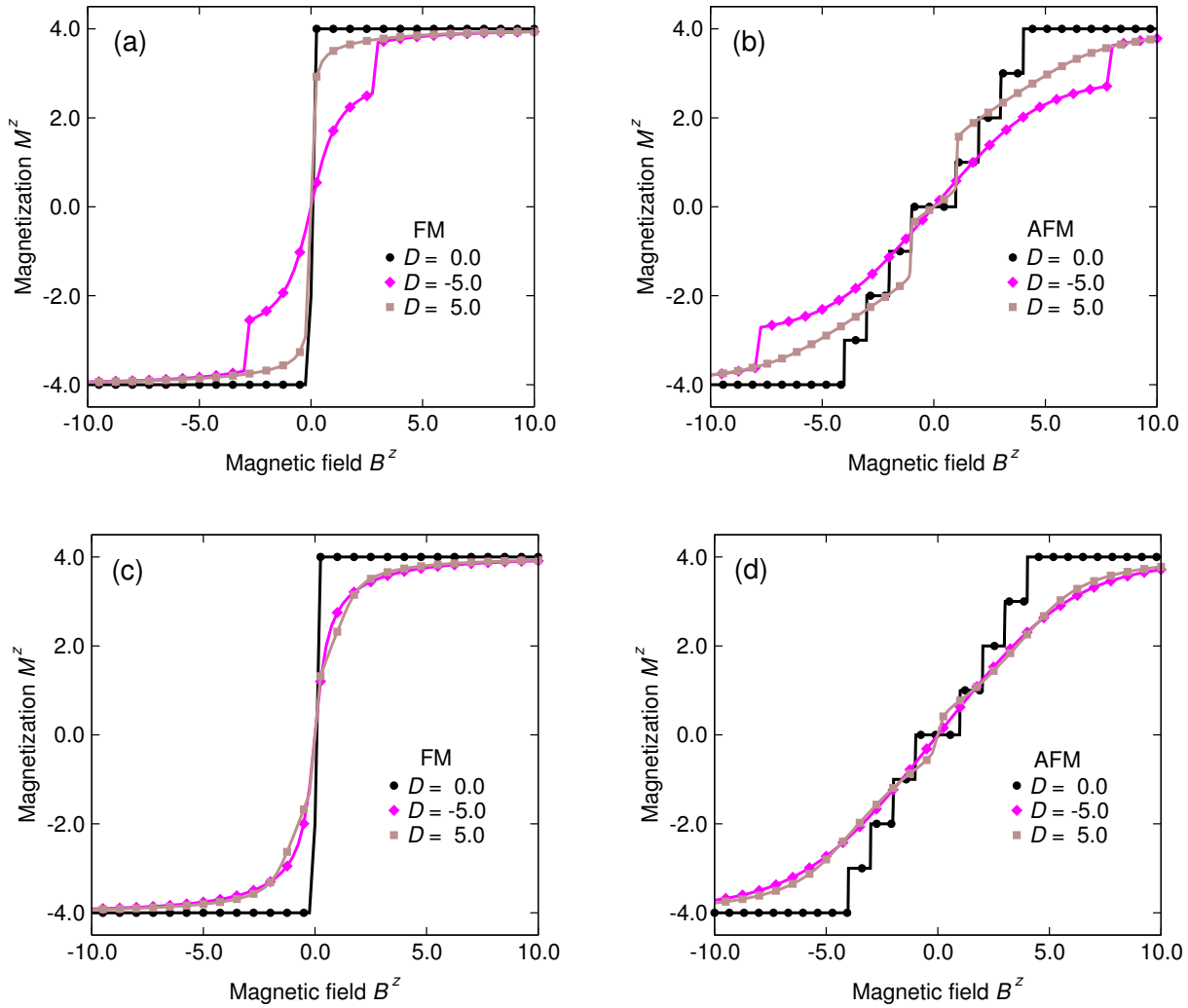

FIG. 10. (Color online) The effect of anisotropy on magnetization as a function of external magnetic field (measured in units of $|J|$) for the spin-1 tetrahedron (a,b) and square (c,d). The results for FM and AFM interactions are shown in the left and right panels, respectively. The black line (circles) shows the variation of magnetization as a function of the magnetic field. The curves with squares (brown) and diamonds (magenta) show the variation of the same quantity for positive and negative D.

are shown for the square and tetrahedron. For the 4-atom spin-1 cluster, the Hamiltonian matrix is of dimension $3^4 \times 3^4$. For $D = 0$, the Hamiltonian matrix can be decomposed into 9 block matrices with $S^z = -4, -3, \ldots, 4$. However, at finite D the block matrix structure is destroyed as the uniaxial anisotropy term does not commute with total S^z and the whole Hamiltonian matrix has to be diagonalized.

The presence of anisotropy D results in a different qualitative behavior of magnetization as a function of the external magnetic field as shown in Fig. 10 for the tetrahedron (a-b) and the square (c-d). In the absence of magnetic anisotropy ($D = 0$), we obtain a single step in the magnetization for FM exchange interaction and 9 plateaus for AFM exchange interaction for both clusters, the tetrahedron and the square. The presence of anisotropy leads to the smearing of magnetization with respect to magnetic field for FM and AFM interactions (see the squares and diamonds) of square and tetrahedron, since $\mathcal{H}_{\rm ani}$ mixes the eigenstates of $\mathcal{H}_0$ with different total spin values. In particular, for tetrahedron geometry, we observe differences in the magnetization for positive and negative values of D, whereas for the square geometry, the change of sign in the anisotropy does not affect the magnetization significantly. This shows the dependence of anisotropy on the structural symmetry, which has been observed earlier for 13-atom clusters through Monte Carlo simulations[34].

In addition, we have calculated the temperature-dependent correlation functions, as defined in Eq. (9), for the 4-atom clusters with spin-1 in the presence of anisotropy. The variation of the nearest-neighbor correlation functions with respect to temperature has been plotted in Fig. 11 for the spin-1 tetrahedron (a-b) and

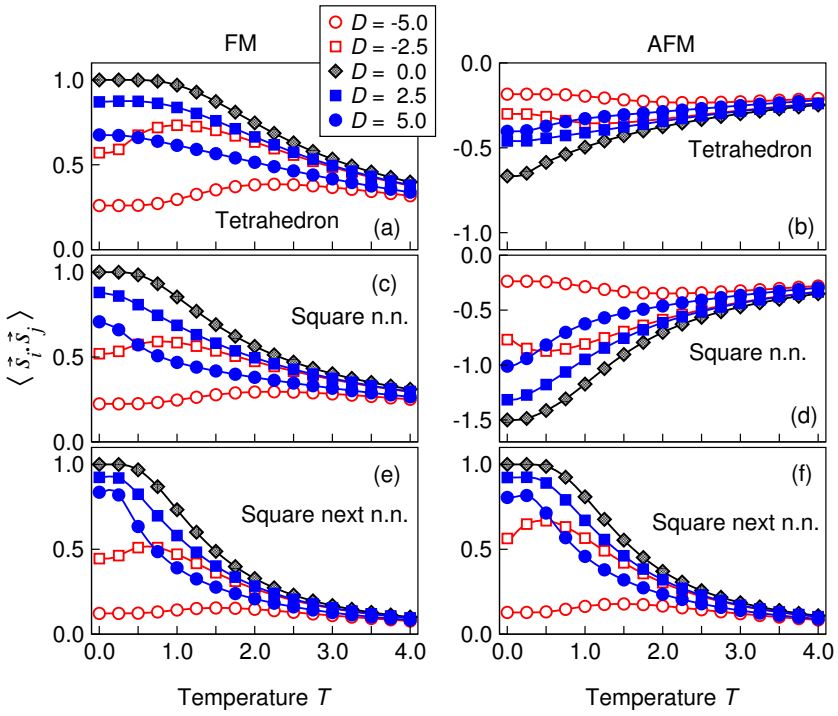

FIG. 11. (Color online) Variation of the spin-spin correlation function with temperature (expressed in units of $|J|$) for the FM and AFM spin-1 tetrahedron (a), (b) and square (c)-(f). Diamonds, open symbols and filled symbols represent the correlation functions $\langle \vec{s}_i \cdot \vec{s}_j \rangle$ for zero, negative and positive anisotropy constants D, respectively.

square (c-f) with different anisotropy constants for the FM (left panel) and AFM (right panel) case. For both interactions, it has been observed that the anisotropy modifies the correlation function significantly at low temperatures. The correlations are positive in the FM cases and negative in the AFM case. For $D \geq 0$ the correlations decrease with temperature as expected. However, for negative D the correlations are reduced at low temperatures due to the quantum effects, as can be seen most easily for the square: Here the classical ground state would be a FM/AFM state in the direction perpendicular to the plane, as in this case all couplings are satisfied and the spin directions are all perpendicular to the anisotropy axes as required. However, $\mathcal{H}_{\rm ani}$ introduces spin-flip process in the system and as a consequence ground state becomes the linear combination of states with different magnetization. Hence a strong reduction in correlations is observed in presence of anisotropy term at low temperatures. This reduction of correlations becomes negligible at higher temperatures, and correlations decrease as usual. While the nearest neighbor correlations in the AFM square (Fig. 11d) are negative, the second nearest neighbor correlations are positive, as the square is not frustrated.

TABLE III. Size of block matrix, lowest energy eigenvalues E_0, ΔE_1, and degeneracies K_0, K_1, for different S^z for 13-atom AFM ICO with spin-1.

$\lvert S^z\rvert$	Matrix size	$E_0/\lvert J\rvert$	K_0	$\Delta E_1/\lvert J\rvert$	K_1
13	1	+42	1	–	–
12	13	+29	1	4.763932	3
11	91	+17	1	4.763932	3
10	442	+10.763932	3	1.236068	5
9	1651	+5.034063	5	0.147456	1
8	5005	−0.131753	4	0.061759	3
7	12727	−4.663902	4	0.032182	5
6	27742	−8.608201	3	0.035204	4
5	52624	−11.932667	4	0.040381	4
4	87802	−14.679508	5	0.011089	3
3	129844	−16.920343	5	0.007569	4
2	171106	−18.566489	3	0.013245	4
1	201643	−19.506298	5	0.007972	5
0	212941	−19.839976	3	0.034983	3

V. SPIN-1 ICOSAHEDRON

Finally we present the results for the spin-1 icosahedron with Hamiltonian described in Eq. (6). Now the Hamiltonian matrix has $3^{13} = 1594323$ columns and rows. For vanishing anisotropy, it can be decomposed into block matrices whose sizes are the trinomial numbers $\binom{13}{k}_2$ for $-13 \leq k \leq 13$, given in Tab. III together with

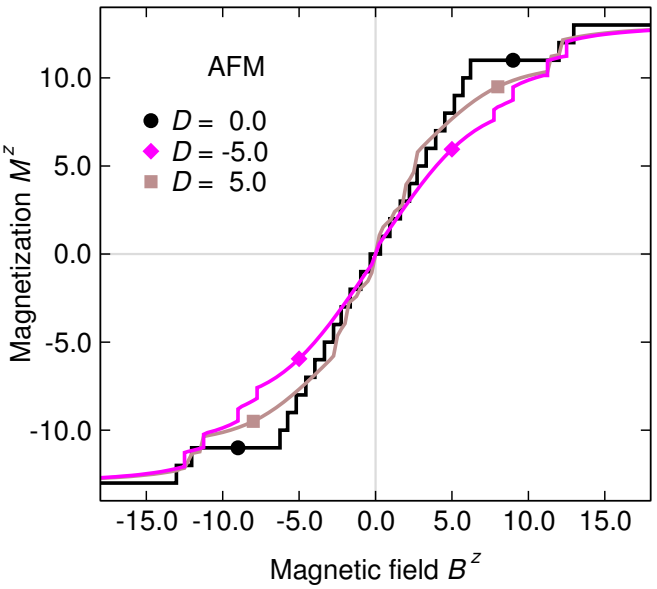

FIG. 12. (Color online) Variation of magnetization M^z as a function of the external magnetic field B^z (measured in units of $|J|$) for different values of the radial uniaxial anisotropy D for the spin-1 AFM icosahedron.

the lowest eigenvalues of each S^z block. From these results we compute the hysteresis curve shown in Fig. 12 as black line. The curve is similar to the spin-1/2 case, since for fields below $|B^z| \lesssim 6$ the magnetization varies with nearly constant step size from -11 to 11. The plateaus at $S^z = \pm 11$ mark the saturated outer shell, where only the central spin still points antiparallel to the external field. At larger fields also $\vec{s}_0$ aligns with the field in two steps, one from $\langle s_0^z \rangle = -1 \to 0$ at $B^z = 12$ and one from $\langle s_0^z \rangle = 0 \to 1$ at $B^z = 13$. This behavior already shows characteristics of the classical limit, in which the steps vanish and the magnetization varies continuously with field. Nevertheless, also in this limit we find a plateau at $M^z = 11$ with reversed central spin, which rotates towards the field direction in the range $11 < B^z < 13$.

The ground state spin correlation functions for the AFM case of ICO with spin-1 are plotted in Fig. 5 (see the filled squares). This shows again similar qualitative behavior to the spin-1/2 case and show antiferromagnetic order in the AFM case, interestingly now the anticorrelation between the third neighbor atoms is larger than the nearest neighbor value. This shows that the correlation approaches towards the classical limit -1, as shown in Fig. 5 (the dashed line). On the other hand, for the FM case, the correlation functions for all shell neighbors become one for the ICO.

Additionally, we have calculated the hysteresis for the icosahedron with radial uniaxial anisotropy according to Eq. (10). For these calculations it was again necessary to work with the whole Hamiltonian matrix, as the anisotropy term does not commute with the interaction term and thus destroys the block structure of $\mathcal{H}$. Nevertheless, we could calculate the smallest eigenvalues and eigenvectors using a Lanczos scheme. The resulting curves are shown in Fig. 12 as magenta ($D = -5$) and brown ($D = +5$) lines, they are similar to the results for the tetrahedron with anisotropy shown in Fig. 10 a,b.

VI. SUMMARY AND OUTLOOK

We have employed the exact diagonalization technique for small spin clusters with 4 and 13 vertices using the quantum-mechanical nearest-neighbor Heisenberg model and calculated the full energy spectrum numerically as well as the ground state energies of the 13-atom systems analytically. The magnetic and thermodynamic properties as well as the spin-spin correlation functions are derived from these results. The ground state magnetization shows discontinuities accompanied by a magnetization plateau as a function of magnetic field for the antiferromagnetic exchange interaction. These magnetization plateaus vanishes for temperatures around $T \gtrsim 0.1|J|$. The ground state correlations suggest that the icosahedron is less frustrated than the cuboctahedron, since a regular $+ - +-$ oscillation is found for the ICO, while the CUBO has irregular correlations with smaller values in the 3rd and 4th neighbor shell, see Fig. 5.

We have shown that the dipolar interaction plays a significant role for the magnetization in case of AFM interaction of the ICO. Our investigations show that dipolar interactions have a strong influence on the magnetization of surface atoms in an external magnetic field, while the field-dependent magnetization of the center atom remains nearly unchanged by the dipolar interactions.

The field dependence of magnetization and temperature dependence of correlation function on tetrahedron and square for $s = 1$ indicates that the influence of radial anisotropies on the magnetic properties strongly depends on the structural symmetry of the cluster.

Finally, we have investigated the 13-atom icosahedron with $s = 1$, which involves quite large Hamiltonian matrices of dimensions $3^{13} \times 3^{13}$ that cannot be decomposed into smaller block matrices if the local uniaxial anisotropy axes are present. Using Lanczos methods we calculated the lowest eigenvalues and corresponding eigenvectors of these large matrices, determined correlation functions and hysteresis curves and compared these results to the spin-1/2 cases.

Regarding any comparison of this exact diagonalization calculation with experiments one has to first of all note that this requires tiny negative exchange coupling to observe the quantum effects (such as steps) in reasonable magnetic field. Nevertheless, there exists few examples in nature such as Mn_{12}-acetate and Mn_4-dimer molecules embedded in organic ligands, which fulfills this condition, see for instance Refs.[1,2]. Another interesting point would be a collection of quantum clusters, showing long-range order at low temperatures. For such calculations, exact

diagonalization results can be used as a basis. This is left for future studies.

ACKNOWLEDGMENTS

One of the authors (A. H.) thank Björn Sothmann for helpful discussions.

[1] D. Gatteschi, R. Sessoli, and J. Villain, *Molecular Nanomagnets* (Oxford university press, Oxford, 2006).
[2] W. Wernsdorfer, N. Aliaga-Alcalde, D. Hendrickson, G. Christou, Nature **416**, 406 (2002).
[3] J. Schnack and M. Luban, Phys. Rev. B **63**, 014418 (2000).
[4] J. J. Henderson, C. M. Ramsey, E. del Barco, T. C. Stamatatos and G. Christou, Phys. Rev. B **78**, 214413 (2008).
[5] R. Schnalle and J. Schnack, Phys. Rev. B **79**, 104419 (2009).
[6] G. Seeber, P. Kögerler, B. M. Kariuki, and L. Cronin, Chem. Commun. (Cambridge) 1580 (2004).
[7] J. Schnack, Dalton Trans. **39**, 4677 (2010).
[8] N. P. Konstantinidis, Phys. Rev. B **72**, 064453 (2005).
[9] Y. Shapira, V. Bindilatti, J. Appl. Phys. **92**, 4155 (2002).
[10] D. Coffey, and S. A. Trugman, Phys. Rev. B **46**, 12717 (1992).
[11] R. Schnalle, A. Laeuchli, and J. Schnack, Condens. Matter Phys. **12**, 331 (2009).
[12] N. P. Konstantinidis, and D. Coffey, Phys. Rev. B **63**, 184436 (2001).
[13] I. Rousochatzakis, A. M. Läuchli, and F. Mila, Phys. Rev. B **77**, 094420 (2008).
[14] N. P. Konstantinidis, Phys. Rev. B **76**, 104434 (2007).
[15] J. Schulenburg, A. Honecker, J. Schnack, J. Richter, and H.-J. Schmidt, Phys. Rev. Lett. **88**, 167207 (2002).
[16] C. Schröder, H.-J. Schmidt, J. Schnack, and M. Luban, Phys. Rev. Lett. **94**, 207203 (2005).
[17] J. Schnack, R. Schmidt, and J. Richter, Phys. Rev. B **76**, 054413 (2007).
[18] J. Schnack, and O. Wendland, Eur. Phys. J. B **78**, 535 (2010).
[19] J. van Slageren, P. Rosa, A. Caneschi, R. Sessoli, H. Casellas, Y. V. Rakitin, L. Cianchi, F. Del Giallo, G. Spina, A. Bino, A.-L. Barra, T. Guidi, S. Carretta, and R. Caciuffo, Phys. Rev. B **73**, 014422 (2006).
[20] O. Ciftja, M. Luban, M. Auslender, and J. H. Luscombe, Phys. Rev. B **60**, 10122 (1999).
[21] O. Ciftja, Physica A **286**, 541 (2000).
[22] D. Coffey, and S. A. Trugman, Phys. Rev. Lett. **69**, 176 (1992).
[23] A. Honecker and M. E. Zhitomirsky, J. Phys. Conference series **145**, 012082 (2009).
[24] S. R. White, Phys. Rev. B **48**, 10345 (1993).
[25] U. Schollwöck, Rev. Mod. Phys. **77**, 259 (2005).
[26] M. P. Gelfand, R. R. P. Singh, and D. A. Huse, J. Stat. Phys. **59**, 1093 (1990).
[27] D. C. Mattis, *The Theory of Magnetism I: Statics and Dynamics* (Springer, New York, 1988).
[28] Q. F. Zhong and S. Sorella, Europhys. Lett. **21**, 629 (1993).
[29] A. E. Trumper, L. Capriotti, and S. Sorella, Phys. Rev. B **61**, 11529 (2000).
[30] A. W. Sandvik and J. Kurkijärvi, Phys. Rev. B **43**, 5950 (1991).
[31] A. W. Sandvik, Phys. Rev. B **59**, R14157 (1999).
[32] L. Engelhardt and M. Luban, Phys. Rev. B **73**, 054430 (2006).
[33] Y. Li, T. Wang, and Y. X. Li, Phys. Status Solidi **247**, 1237 (2010).
[34] L. Hernández and C. Pinettes, J. Magn. Magn. Mater. **295**, 82 (2005).
[35] Z. B. Li, K. L. Yao, and Z. L. Liu, J. Magn. Magn. Mater. **320**, 1759 (2008).
[36] C. Herring, in *Magnetism*, edited by G. T. Rado and H. Suhl (Academic, New York, 1996).
[37] F. Bonechi, E. Celeghini, R. Giachetti, E. Sorace, and M. Tarlini, J. Phys. A: Math. Gen. **25**, L939 (1992).
[38] H. Q. Lin and J. E. Gubernatis, Computers in Physics **7**, 401 (1993).
[39] D. Gatteschi and L. Pardi, Gazz. Chim. Ital. **123**, 1 (1993).
[40] J. J. Borrás-Almenar, J. M. Clementa-Juan, E. Coronado, and B. S. Tsukerblat, Inorg. Chem. **38**, 6081 (1999).
[41] B. S. Tsukerblat, *Group Theory in Chemistry and Spectroscopy: A Simple Guide to Advanced Usage*, (Dover publications, Mineola, New York, 2006).
[42] R. Schnalle and J. Schnack, Int. Rev. Phys. Chem. **29**, 403 (2010).
[43] V. E. Sinitsyn *et al.*, J. Phys. A: Math. Theor. **40**, 645 (2007).
[44] H. W. Kroto, J. R. Heath, S. C. O'Brien, R. F. Curl, and R. E. Smalley, Nature **318**, 162 (1985).
[45] P. W. Fowler and D. E. Manolopoulos, *An Atlas of Fullerenes* (Oxford University Press, London, 1995).
[46] S. L. Altmann and P. Herzig, *Point-Group Theory Tables* (Oxford University Press, London, 1994).
[47] G. Rollmann, M. E. Gruner, A. Hucht, R. Meyer, P. Entel, M. L. Tiago, and J. R. Chelikowsky, Phys. Rev. Lett. **99**, 083402 (2007)
[48] *Mathematica* 8.0, Wolfram Research, Inc., Champaign, Illinois, (2010).
[49] D. J. Breed, Physica **37**, 35 (1967).
[50] S. Sahoo, A. Hucht, M. E. Gruner, G. Rollmann, P. Entel, A. Postnikov, J. Ferrer, L. Fernández-Seivane, M. Richter, D. Fritsch, and S. Sil, Phys. Rev. B **82**, 054418 (2010).
[51] G. Kamieniarz, R.W. Gerling, L.S. Campana, A. Caramico D'Auria, F. Esposito, and U. Esposito, J. Magn. Magn. Mater. **104**, 865 (1992).
[52] R. A. Klemm and D. V. Efremov, Phys. Rev. B **77**, 184410 (2008).